Biaxial nematic order and phase behavior studies in an organosiloxane tetrapode using complementary deuterium NMR experiments

C. Cruz,[1,2] J. L. Figueirinhas,[1,2] D. Filip,[1,3] G. Feio,[1,4] A. C. Ribeiro,[1,2] Y. Frère,[5] T. Meyer,[6] and G. H. Mehl[6]
[1]*CFMC-UL, Av. Prof. Gama Pinto 2, 1649-003 Lisboa, Portugal*
[2]*IST, Av. Rovisco Pais, 1049-001 Lisboa, Portugal*
[3]*"Petru Poni" Institute of Macromolecular Chemistry, Aleea Gr. Ghica Voda 41 A, 700487-Iasi, Romania*
[4]*CENIMAT, Faculdade de Ciências e Tecnologia, Universidade Nova de Lisboa, 2829-516 Caparica, Portugal*
[5]*Institut Charles Sadron, UPR22-CNRS, 6, rue Boussingault-BP 40016, F-67083 Strasbourg Cedex, France*
[6]*Department of Chemistry, The University of Hull Cottingham Road, Hull, HU6 7RX, United Kingdom*
(Received 10 May 2006; revised manuscript received 10 July 2008; published 12 November 2008)

The biaxial nematic phase was recently observed in different thermotropic liquid crystals, namely bent-core compounds, side-chain polymers, bent-core dimers, and organosiloxane tetrapodes. In this work, a series of experiments with a nematic organosiloxane tetrapode where nuclear magnetic resonance (NMR) spectra are collected while the sample is continuously rotating around an axis perpendicular to the magnetic field, are discussed in conjunction with the analysis of a deuterium NMR experiment on the same system reported earlier. The sample used is a mixture of a deuterated probe with the tetrapode. The mixture exhibits a nematic range between −40 °C and 37 °C. The results of the two independent, but complementary deuterium NMR experiments confirm the existence of a biaxial nematic phase for temperatures below 0 °C with high values of the asymmetry parameter at low temperatures. The presence of slow movements of the tetrapode mesogenic units in the low-temperature regime could also be detected through the analysis of the NMR spectra. Simulations indicate that these movements are mainly slow molecular reorientations of the mesogenic units associated with the presence of collective modes in the nematic phases of this compound. In the case of tetrapodes, recent investigations attribute the origin of biaxiality to the hindering of reorientations of the laterally attached mesogenic units which constitute the tetrapode. This study relates the molecular movements with the nematic biaxial ordering of the system.

DOI: 10.1103/PhysRevE.78.051702 PACS number(s): 61.30.Cz, 61.30.Eb

I. INTRODUCTION

After a long quest for the elusive nematic biaxial (N_b) phase in thermotropic liquid crystals [1–3], it has recently been reported to appear in a number of systems, namely bent-core compounds [4], side-chain polymers [5], bent-core dimers [6], and organosiloxane tetrapodes [7,8]. Considering the potential applications of these systems and their relevance from the fundamental point of view, the search for compounds exhibiting the N_b phase is a very topical issue [2]. Nematic biaxiality has also been theoretically predicted for other systems such as mixtures of calamitic and/or discotic molecules with linked rod-plate amphiphiles [9–13]. Very recently, for tetrapode systems, the biaxial nematic phase was predicted in the form of a cubatic phase [14]. In this paper, the results of two independent deuterium NMR experiments, showing the existence of a N_b phase in an organosiloxane tetrapode are reported.

Liquid crystalline organosiloxane tetrapodes are a particular case of dendritic molecules (generation 0 dendrimers) [15] formed by four mesogenic units linked to the central silicon by a relatively flexible chain. In the material studied (see molecular structure in Fig. 1), the aromatic mesogenic units are connected to the central core by a laterally attached chain. A molecular packing model involving an interdigitation of the mesogenic units, schematically depicted in Fig. 2, conforms with the fundamental entropic and steric requirements for the biaxial nematic phase [16–18]. The structure of this mesophase and the extension of the nematic phase, ranging to very low temperatures, influence the molecular order as is clearly shown by the NMR results and will be discussed in detail in Sec. IV B. One of the fundamental questions to be addressed is how molecular structure and nematic phase biaxiality can be correlated.

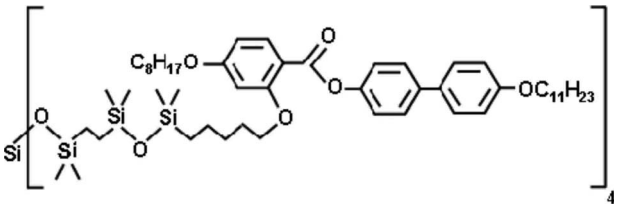

Pure compound

$$T_g \xrightarrow{-30°C} N_B \xrightarrow{37°C} N_U \xrightarrow{47°C} I$$

Mixture with 7CBαd2 (probe - 15% weight)

$$T_g \xrightarrow{-40°C} N_B \xrightarrow{0°C} N_U \xrightarrow{37°C} I$$

FIG. 1. Molecular structure and phase sequence of the organosiloxane tetrapode which exhibits the biaxial nematic phase both for the pure compound and the mixture with deuterated liquid crystal 7CBαd2. N_U-N_B transitions temperatures quoted from this work and Refs. [7,8].

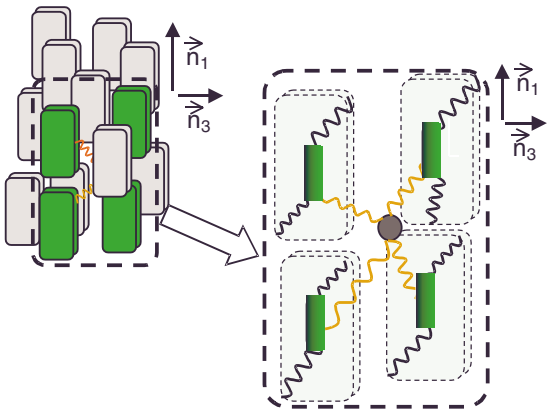

FIG. 2. (Color online) Schematic representation of structure of the nematic phase formed by the tetrapodes.

The structure of the commonly observed uniaxial nematic mesophase is characterized by a single direction defined by a unit vector (the director) $\boldsymbol{n}$, corresponding to the preferential alignment of the long axis of the mesogenic units. These units are individual molecules in the case of low molecular weight liquid crystals or rigid anisometric molecular segments connected to the backbone in the case of liquid crystal polymers or to a dendritic core in the case of liquid crystal dendrimers [19]. The biaxial nematic phase, contrary to the uniaxial one, is characterized by an additional direction of preferential molecular alignment in the plane perpendicular to the main director, $\boldsymbol{n}_1$, (see Fig. 2) and is described by secondary directors, $\boldsymbol{n}_2$ and $\boldsymbol{n}_3$. Therefore, molecules or mesogenic units presenting a certain degree of molecular biaxiality could be expected to favor the appearance of the N_b phase. Actually, this condition is present to some extent in most liquid crystal (LC) molecules but it is not sufficient to give rise to a biaxial nematic mesophase. The unrestricted rotation around the long molecular axis usually leads to uniaxial symmetry.

A biaxial mesophase may be identified by measuring a macroscopic physical property characterized by a second rank tensorial quantity $\boldsymbol{Q}$. The asymmetry parameter is defined as $\eta=\frac{Q_{yy}-Q_{xx}}{Q_{zz}}$, where Q_{ii} are the principal values of the tensor labeled to fulfill the condition $|Q_{zz}|>|Q_{yy}|\geqslant|Q_{xx}|$. η will be finite in the biaxial phase and zero in the uniaxial one. In the case of the biaxial phase, the x and y axis define the secondary directors $\boldsymbol{n}_2$ and $\boldsymbol{n}_3$ which are degenerate in the uniaxial phase. To avoid possible effects of surface interactions on the alignment of the mesophase (which could lead to additional ordering resulting from confinement and not from the phase itself) the analysis of biaxiality is more conclusive when performed in a bulk sample. This is the case for deuterium NMR measurements, where the average electric field gradient, (AFG), corresponding to the C-D bond in a molecule is detected. Using this technique, the question of biaxiality in the nematic phase was recently clarified for several liquid crystalline systems [2,4,20,21]. This procedure is based on the assumption that the principal frame of the AFG tensor resulting from the molecular ensemble coincides to that of the tensorial order parameter Q and the components of both tensors are proportional.

In the case of a polydomain sample, the NMR signal corresponds to a superposition of contributions coming from the different domains and a so-called powder spectrum is obtained as will be discussed further in the next sections. The order parameters measured from a polydomain sample correspond to those of the domains and the distinction between local order and phase order depends on the domains size. This difference is not directly observed by a NMR experiment on a polydomain unless some additional information on domains size is obtained either through modelling or other means, for instance, from optical techniques. In biaxial phases the secondary directors lose the degeneracy they have in uniaxial phases and consequently the detection of partial or total alignment of the secondary directors by the static magnetic field can also be used to confirm the presence of phase biaxiality, as in the case of experiments on rotating samples where a two-dimensional powder on the main director coexist with the alignment of one of the secondary directors.

In the present case, a low molecular weight uniaxial nematic liquid crystal was used as a deuterated probe mixed with the tetrapode compound. Two types of independent experiments were performed for the study of the biaxial ordering in the system: One where the acquisition of the NMR spectra follows a 90° rotation of the sample around one axis perpendicular to the static magnetic field (starting from an aligned situation) and a second where the NMR data are collected while the sample rotates continuously around the same axis. Both methods have previously been used to detect biaxiality in nematic and other LC phases such as SmC, SmF, and SmG [2,4,8,22,23]. In principle, both of these techniques allow for the determination of the asymmetry parameter and of the quadrupolar coupling constant. The data obtained with both methods in this study was analyzed coherently to determine values for the asymmetry parameter and the quadrupolar coupling constant at each temperature measured. These results confirm the existence of a biaxial nematic phase on a polydomain sample where the secondary directors are partially aligned for temperatures below 273 K as reported earlier [8] where just one of these methods was used. The results are discussed considering the hindering of local fast molecular reorientations of the mesogenic units correlated to the asymmetry of the interactions between the mesogenic cores [8]. Furthermore, the consistent analysis of the NMR results obtained in the case of the continuous sample rotation allowed for the detection of slow reorientational motions of the mesogenic units associated with the collective modes of the nematic phase [16,24,31].

II. EXPERIMENT

A. Description of the system studied

The investigated material is an organosiloxane tetrapode (molecular mass 3597.96 g mol^{-1}) based on a siloxane core linked to four aromatic mesogens, each of which terminated by C_8 and C_{11} alkyl chains, respectively. The flexible spacers which link the mesogens to the siloxane core are formed by five methylene groups and tetramethyldisiloxane groups. The synthesis of the material has been described elsewhere [25].

The sample used for ^{2}H NMR measurements is a mixture consisting of the tetrapode compound (85% weight) and the nematic liquid crystal 7CBαd2, used as a deuterated probe (15% by weight).

It is noted that implicit in all experiments is the fundamental assumption that the probe records truthfully the phase behavior of the host. Thus, a mesogenic probe was selected which, due to its chemical structure, would be located preferentially in the vicinity of the aromatic groups. It was judged crucial for the probe to be nematic, as this would lead to strong van der Waals interactions between the aromatic groups of the probe and aromatic rings of the mesogens considered to be responsible for the biaxial nematic phase behavior. Or, in other words, it was necessary to ensure that the phase structure built up by the aromatic rings system is measured with a probe which could interact strongly with those groups. It is noted here that unsuitable probes can be positioned in the much less ordered alkyl chains. Earlier investigations on the biaxiality of the SmF and the SmG phases exhibited by compounds with molecules deuterated in different sites clearly showed that the detected asymmetry parameters depend strongly on the position of deuterium in the molecule [23,26].

The pure tetrapode compound exhibits a nematic phase in a broad temperature domain (between −30 °C and 47 °C). In the mixture, the thermal domain of the nematic phase is shifted to −40 °C to 37 °C as confirmed by polarizing optical microscopy (POM) and differential scanning calorimetry (DSC) measurements. The molecular structure of the tetrapode as well as the phase sequences of the pure compound and the mixture are presented in Fig. 1.

B. NMR measurements

NMR measurements were performed in a BRUKER MSL 300 spectrometer using a quadrupolar echo pulse sequence [27] with phase cycling. The sample consisted of a few hundred milligrams of the mixture of the tetrapode with the deuterated probe in a sealed NMR glass tube with a diameter of 7 mm. The temperature was controlled within ±0.1 °C using an Eurotherm B-VT2000 controller with liquid nitrogen cooling and nitrogen circulation.

Two types of independent experiments were performed: (i) Acquisition of the NMR spectra following a 90° rotation of the sample around an axis perpendicular to the static magnetic field (starting from an aligned situation); (ii) acquisition of NMR data while the sample rotates continuously around the same axis.

In both experiments (i) and (ii), the spectra from the aligned sample were first recorded after the sample had been slowly cooled down from the isotropic phase to the measuring temperature and prior to sample rotation. These spectra are used as a reference in comparison with those of the rotated sample.

In experiment (i) the data was collected while maintaining the sample rotated at 90° relative to the initial alignment for short periods of time (up to 30 s), followed by rotating the sample back to 0° for up to 150 s, and this process was repeated to obtain data sets with suitable signal-to-noise ratios. This technique was used to prevent the realignment of the nematic principal director considering that, for the material under study and the available experimental conditions, the minimum $\boldsymbol{n}_1$ reorientation times are of the order of a few minutes (for the highest temperatures). The ideal situation to identify a biaxial nematic phase would correspond to a perfect alignment of the secondary directors due to the NMR static magnetic field during the observation periods where the main director is tilted. This desired scenario corresponds to the realization of a perfect monodomain sample. However, specific experimental conditions and materials' physical properties may impose limitations to the attainability of such a favorable ideal condition. The concretization of this desired situation depends mainly on the anisotropy of the magnetic susceptibility in the plane perpendicular to $\boldsymbol{n}_1$, the viscosities of the material and the intensity of the static magnetic field. The magnetic susceptibility anisotropy must be high enough and the rotational viscosity low enough to allow the secondary directors to align in the experimental conditions determined by the material and the spectrometer used. Actually, as will be discussed later, the desired ideal configuration was only partially obtained.

In experiment (ii) spectra were collected while the sample was rotating continuously with a frequency of 0.735 rotations/second (44.1 rpm). The continuous rotation of the sample around one axis perpendicular to the NMR static magnetic field $\boldsymbol{B}_0$, with a speed above a certain limit may generate a distribution of the $\boldsymbol{n}_1$ director. In the case generally considered in the literature [22] a two-dimensional powder pattern is formed as $\boldsymbol{B}_0$ lies distributed with equal probability in the plane defined by $\boldsymbol{n}_1$ and $\boldsymbol{n}_2$ [4,22,40] in the frame of the rotating sample. The case described above [4,22,40] implies a perfect alignment of one of the secondary directors ($\boldsymbol{n}_3$) of the biaxial nematic domains with the axis of the sample rotation. As will be discussed in Sec. IV A 2, this ideal situation is not attained in the present work due to specific experimental conditions related mainly with the material's viscosity. Nevertheless, the measurement of the order parameters may be achieved through a careful data analysis procedure of the spectra collected from both the 90° rotated samples and the continuously rotating samples.

III. NMR THEORY

A. Spectrum of a static distribution

In an aligned nematic domain with positive magnetic susceptibility anisotropy, the main director $\boldsymbol{n}_1$ is parallel to the NMR static magnetic field $\boldsymbol{B}_0$. Due to symmetry reasons, it is assumed that (in the biaxial nematic) the aligned sample consists of a number of biaxial nematic domains with $\boldsymbol{n}_1$ parallel to $\boldsymbol{B}_0$ and secondary directors ($\boldsymbol{n}_2$ and $\boldsymbol{n}_3$) uniformly distributed in the plane perpendicular to $\boldsymbol{n}_1$ (see Fig. 2). In each biaxial domain, the orientation of $\boldsymbol{B}_0$ relative to the principal frame defined by $\boldsymbol{n}_1$, $\boldsymbol{n}_2$, and $\boldsymbol{n}_3$ is given by the Euler angles θ and φ which, for $\boldsymbol{B}_0$ aligned with $\boldsymbol{n}_1$, assume the values $\theta=0$ and φ undetermined. The rotation of the aligned sample around an axis perpendicular to $\boldsymbol{B}_0$ of a finite angle results in a particular angle θ between $\boldsymbol{n}_1$ and $\boldsymbol{B}_0$ and a different φ angle for each domain resulting from the original distributed

orientation of the secondary directors which may eventually change due to the interaction of the rotated domains', with a given magnetic susceptibility with $\boldsymbol{B}_0$. Ideally, as discussed before, the angles φ corresponding to different domains will coincide after the rotation, giving rise to a nematic monodomain.

In general, the domain distribution in the rotated sample is equivalent to a distribution of orientations of the magnetic field $\boldsymbol{B}_0$ given by $P(\Omega)$ $[\Omega \equiv (\theta, \varphi)]$, where θ and φ are the Euler angles defining the orientation of $\boldsymbol{B}_0$ in the frame defined by $\boldsymbol{n}_1$, $\boldsymbol{n}_2$, and $\boldsymbol{n}_3$ for each domain. This frame is considered to coincide with the principal frame of the averaged field gradient (AFG) tensor $\bar{\mathbf{V}}$ associated with each domain. The deuterium NMR spectra of such a sample, $G(\omega)$, will result from the sum of contributions of pairs of absorption lines $L(\omega)$ corresponding to the different nematic domains,

$$G(\omega) = \int_{\Omega} \left[L\left(\omega - \frac{\delta\omega}{2}\right) + L\left(\omega + \frac{\delta\omega}{2}\right) \right] P(\Omega) d\Omega. \quad (1)$$

Each of these pairs of lines has a frequency splitting given by

$$\delta\omega = \frac{3\pi}{2} \bar{\nu}_Q [(3\cos^2\theta - 1) + \eta \sin^2\theta \cos 2\varphi], \quad (2)$$

where $\bar{\nu}_Q$ is the averaged quadrupolar coupling constant and η is the asymmetry parameter. As defined earlier for a general second-rank tensorial quantity, the asymmetry parameter is given in this case by

$$\eta = \frac{\bar{V}^{XX} - \bar{V}^{YY}}{\bar{V}^{ZZ}}, \quad (3)$$

where $\bar{V}^{ii}$ are the principal values of the averaged field gradient tensor in a nematic domain.

The ^{2}H spectrum observed will be determined by the averaged quadrupolar coupling constant, $\bar{\nu}_Q$, the asymmetry parameter, η, and the domain distribution $P(\Omega)$ resulting from the particular experimental conditions. The analysis of the experimental results is carried out by fitting expression (1) to each spectrum, considering an appropriate line-shape expression given by $L(\omega)$. As a result, the fitting parameters $\bar{\nu}_Q$ and η are obtained. If the ideal situation mentioned above of perfect alignment of secondary directors is attained, the resulting order parameters, and in particular the asymmetry parameter η may be directly related with the whole nematic monodomain. In that case, it will be straightforward to identify these order parameters as characteristics of the phase. On the other hand, it is important to stress that, if the analyzed spectra correspond to a polydomain sample, the measurement of a nonzero asymmetry parameter is a necessary but not a sufficient condition to the identification of the phase as a biaxial nematic phase. An isolated measurement of a η parameter different from zero in a polydomain sample merely confirms the existence of a locally rhombic order tensor. In that case the identification of macroscopic biaxial ordering properties must be concurrently achieved by additional observations of partial or total orientation of the secondary directors or observations by other experimental techniques, for instance, by optical means [28]. If the nematic domains in the sample are much larger than the molecular dimensions, implying the existence of long-range correlations of the transversal molecular orientations, then it will be possible to consider the measurement of nonzero η as an evidence of biaxial nematic phase ordering.

B. The effect of slow motions

The approach presented in Sec. III A is valid in a regime where the molecular movements are much faster than the NMR observation time ("fast motion regime"). In that case, the ^{2}H spectrum is determined by an averaged electric field gradient tensor (associated with the C-D bonds) resulting from the fast movements of the molecules. When the C-D bonds are moving slowly enough so that the molecular reorientation correlation time falls within the time scale of the NMR observation, a specific approach must be considered in the calculation of the theoretical spectra [29]. A more general approach based on the stochastic Liouville equation has also been put forward to analyze a similar problem [30]. Molecular dynamics of liquid crystals is characterized by movements of different time scales, corresponding to a very broad frequency range (from Hz to hundreds of MHz) [31]. In the present case, the movements with time scale comparable to τ (see (4) below) which correspond typically to collective modes, are those that will more significantly affect the NMR spectra.

Taking into account that the quadrupolar echo pulse sequence was used in the experiments described in this paper, the spectrum associated to a single biaxial nematic domain $F(\omega)$ is given by the Fourier transform of the free induction decay signal $f(t)$ corresponding to this pulse sequence [29],

$$f(t,\Omega) \propto \mathrm{Re}\left\langle \exp\left\{ i \int_{\tau}^{t+2\tau} \omega_0[\Omega, t', \vec{r}] dt' - i \int_0^{\tau} \omega_0[\Omega, t', \vec{r}] dt' \right\} \right\rangle, \quad (4)$$

where Re stands for the real part of, the brackets $\langle \cdots \rangle$ indicate an ensemble average, τ is the delay between rf pulses in the solid echo sequence and ω_0 is the time-dependent absorption frequency of the nuclear spins at time t' at $\vec{r}$ given by [29]

$$\omega_0(\alpha_1, \alpha_2, t', \vec{r}) = \frac{3\pi}{\sqrt{6}} \frac{eQ}{h} \sum_{m=-2,n=-2}^{2,2} \mathrm{D}^2_{m,0}(\alpha_2, \pi/2, 0) \times \mathrm{D}^2_{n,m}(\alpha_1, \pi/2, \pi/2) V_n(t', \vec{r}) \quad (5)$$

where e is the electron charge, Q is the quadrupolar moment of the deuterium nucleus, h is the Planck constant, D^2_{ij} are the components of the 2° rank Wigner rotation matrices [32], V_n are the irreducible components of the time-dependent electric field gradient tensor in the nematic domain at position $\vec{r}$, and the angles α_1 and α_2 define the orientation of the static field $\boldsymbol{B}_0$ in the principal frame of the average electric field gradient tensor in the nematic domain as shown in Fig. 3. In a polydomain sample with a distribution of orientations $P(\Omega)$, the resulting spectrum will be given by

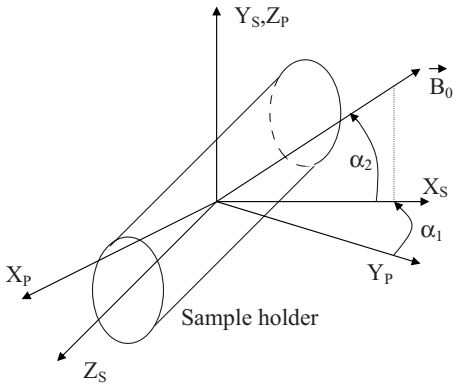

FIG. 3. Definition of the angles α_1 and α_2 that define the orientation of the magnetic field in the principal frame of the averaged electric field gradient tensor associated with each nematic domain (frame P). Frame S is fixed with the NMR sample holder and may rotate in the laboratory, its position relative to the static field $\mathbf{B}_0$ is defined by the angle α_2.

$$G(\omega) = FT[g(t)], \quad \text{with } g(t) = \int f(t,\Omega)P(\Omega)d\Omega. \tag{6}$$

Expression (4) for $f(\Omega,t)$ can be further evaluated considering that ω_0 is a Gaussian random variable due to the fluctuations affecting V_n and, consequently, the argument of the exponential in (4) is also a random variable of the same type. Defining X as the argument of the exponential in (4), $X \equiv \int_{\tau}^{t+2\tau}\omega_0[\Omega,t',\vec{r}]dt' - \int_0^{\tau}\omega_0[\Omega,t',\vec{r}]dt'$, $f(t,\Omega)$ becomes

$$f(t,\Omega) \propto \mathrm{Re}\{\langle \exp[iX]\rangle\}, \tag{7}$$

that evaluates to [29]

$$f(t,\Omega) \propto \mathrm{Re}\left[\exp[i\langle X\rangle]\exp\left(-\frac{\langle (X-\langle X\rangle)^2\rangle}{2}\right)\right]. \tag{8}$$

To proceed in the calculation of $f(t,\Omega)$, the expectation values $\langle X\rangle$ and $\langle (X-\langle X\rangle)^2\rangle$ must be evaluated. Defining $G_n(\Omega) \equiv \Sigma_{m=-2}^{2} D_{m,0}^{2}(\alpha_2,\pi/2,0)D_{n,m}^{2}(\alpha_1,\pi/2,\pi/2)$, $\langle X\rangle$ is readily obtained,

$$\langle X\rangle = \langle \omega_0(\Omega,t',\vec{r})\rangle t = t\frac{3\pi}{\sqrt{6}}\frac{eQ}{h}\sum_{n=-2}^{2} G_n(\Omega)\langle V_n(t',\vec{r})\rangle. \tag{9}$$

To evaluate $\langle (X-\langle X\rangle)^2\rangle$ we consider the correlation function $g(t') \equiv \langle \omega(\Omega,0,\vec{r})\omega(\Omega,t',\vec{r}')\rangle$ where $\vec{r}\prime$ is the position at time $t\prime$ of the spins located at $\vec{r}$ for $t=0$ due to translational diffusion. Using the definition of X we obtain

$$\begin{aligned}\langle (X-\langle X\rangle)^2\rangle = 2\Bigg(&\int_0^t (t-u)g(u)du + \int_0^t dv\int_{\nu}^{\nu+\tau} g(u)du \\ &- \int_0^t dv\int_{\nu+\tau}^{\nu+2\tau} g(u)du\Bigg) + 4\int_0^{\tau}(\tau-u)g(u)du \\ &- \left(\int_0^{\tau} ug(u)du + \int_{\tau}^{2\tau}(2\tau-u)g(u)du\right) \\ &- [\langle \omega_0(\Omega,t',\vec{r}')\rangle t]^2.\end{aligned} \tag{10}$$

From its definition the correlation function $g(t')$ is given by

$$g(t') = \left(\frac{3\pi}{\sqrt{6}}\frac{eQ}{h}\right)^2 \sum_{n,l=-2}^{2} G_n(\Omega)G_l(\Omega)\langle V_n(0,\vec{r})V_l(t',\vec{r}')\rangle \tag{11}$$

the determination of both $\langle V_n(t',\vec{r}')\rangle$ and $\langle V_n(0,\vec{r})V_1(t',\vec{r}')\rangle$ completes the calculation of $f(\Omega,t)$. This will be accomplished considering that the electric field gradient tensor averaged over the fast motions at each point $\vec{r}$ in the nematic domain should be proportional to the order parameter tensor at that point,

$$V_n(t',\vec{r}') = cQ_n(t',\vec{r}'), \tag{12}$$

where c is a constant and Q_n is the nth irreducible component of the tensor order parameter. We separate $Q_n(t',\vec{r}')$ in its average value in the nematic domain plus a fluctuating part dominated by the collective modes as follows:

$$Q_n(t',\vec{r}') = Q_n^0 + \Delta Q_n(t',\vec{r}') \tag{13}$$

with Q_n^0 given in its principal frame by $Q_{\pm 2}^0 = \frac{\eta S}{2}$, $Q_{\pm 1}^0 = 0$, $Q_0^0 = \frac{\sqrt{6}}{2}S$, where η is the asymmetry parameter and S the nematic order parameter. S and η are fitting parameters in the model.

This yields for $V_n^0 \equiv \langle V_n(t',\vec{r}')\rangle$,

$$V_n^0 = cQ_n^0, \tag{14}$$

and for $\langle X\rangle$,

$$\langle X\rangle = \langle \omega_0(\Omega,t',\vec{r}')\rangle t = t\frac{3\pi}{\sqrt{6}}\frac{eQ}{h}c\sum_{n=-2}^{2} G_n(\Omega)Q_n^0. \tag{15}$$

The constant c can be calculated from Eq. (14) and considering the $n=0$ component, it is given by

$$c = \frac{V_0^0}{Q_0^0} = \frac{V_{zz}^0}{S} = \frac{h}{eQ}\frac{\nu_Q}{S} = \frac{h}{eQ}\frac{\nu_{QS}}{1} \tag{16}$$

with $\nu_{QS}=70.05$ kHz estimated from ν_Q in the solid state associated with the α position of the aliphatic chain (170 kHz) [33] and the orientation of the most ordered axis relative to the para-axis of benzene rings in the probe molecule core.

The correlation function $\langle V_n(0,\vec{r})V_1(t',\vec{r}')\rangle$ now becomes

$$\langle V_n(0,\vec{r})V_1(t',\vec{r}')\rangle = c^2[Q_n^0Q_l^0 + \langle \Delta Q_n(0,\vec{r})\Delta Q_l(t',\vec{r}')\rangle]. \tag{17}$$

It is now convenient to express the fluctuating part of the tensor order parameter Q in Cartesian components and as Q is symmetric and traceless only five of them are independent. Labeling them ΔQ_1^c to ΔQ_5^c according to

$$\Delta Q^c = \begin{bmatrix} -\frac{1}{2}(\Delta Q_1^c - \Delta Q_2^c) & \Delta Q_3^c & \Delta Q_4^c \\ \Delta Q_3^c & -\frac{1}{2}(\Delta Q_1^c + \Delta Q_2^c) & \Delta Q_5^c \\ \Delta Q_4^c & \Delta Q_5^c & \Delta Q_1^c \end{bmatrix}, \tag{18}$$

the irreducible components of ΔQ are given by

$$\Delta Q_n = \sum_{j=1}^{5} C_{nj} \Delta Q_j^c, \tag{18a}$$

where C is a 5×5 complex matrix defined by the relation between the irreducible and Cartesian components of a second rank traceless symmetric tensor [29].

The correlation function in (17) $\langle \Delta Q_n(0,\vec{r}) \Delta Q_l(t',\vec{r}') \rangle$ becomes

$$\langle \Delta Q_n(0,\vec{r}) \Delta Q_l(t',\vec{r}') \rangle = \sum_{j,k=1}^{5} C_{nj} C_{lk} \langle \Delta Q_j^c(0,\vec{r}) \Delta Q_k^c(t',\vec{r}') \rangle. \tag{19}$$

We then consider the representation of $\Delta Q_n^c(t',\vec{r}\,')$ as a spatial Fourier series to obtain from (17),

$$\langle V_n(0,\vec{r}) V_1(t',\vec{r}') \rangle$$

$$= c^2 \left(Q_n^0 Q_l^0 + \sum_{j,k=1}^{5} C_{nj} C_{lk} \sum_{\vec{q},\vec{q}'} \langle \Delta Q_j^c(0,\vec{q}) \Delta Q_k^c(t',\vec{q}') \rangle e^{i(\vec{q}.\vec{r}+\vec{q}'.\vec{r}')} \right) \tag{20}$$

and as the Fourier components for different wave vectors are uncorrelated, we get

$$\langle V_n(0,\vec{r}) V_1(t',\vec{r}') \rangle = c^2 \left(Q_n^0 Q_l^0 + \sum_{j,k=1}^{5} C_{nj} C_{lk} \sum_{\vec{q}} \langle \Delta Q_j^c(0,\vec{q}) \Delta Q_k^{c*}(t',\vec{q}) e^{i\vec{q}.(\vec{r}-\vec{r}')} \rangle \right). \tag{21}$$

The expectation value on the right-hand side of Eq. (21) is given by

$$\langle \Delta Q_j^c(0,\vec{q}) \Delta Q_k^{c*}(t',\vec{q}) e^{i\vec{q}(\vec{r}-\vec{r}')} \rangle$$

$$= \langle \Delta Q_j^c(0,\vec{q}) \Delta Q_k^{c*}(t',\vec{q}) \rangle \int_V \int_V P(\vec{r}',\vec{r},t') P_0(\vec{r}) e^{i\vec{q}(\vec{r}-\vec{r}')} dr^3 dr'^3 \tag{22}$$

assuming that the diffusion process is independent of the order parameter fluctuations [34]. V is the domain volume, $P_0(\vec{r})$ is the positional probability density for a spin in the nematic domain at $t=0$ and is just V^{-1} and $P(\vec{r}',\vec{r},t')$ is the conditional positional probability density for a spin to be inside the volume element dr'^3 located at $\vec{r}'$ for $t=t'$ when it was located at $\vec{r}$ for $t=0$. $P(\vec{r}',\vec{r},t')$ is approximated by the solution of the diffusion equation (23) in the domain volume V, where the anisotropy of the nematic medium has been neglected in order to simplify the analysis and limit the number of model parameters

$$\frac{\partial P}{\partial t} = D\Delta^2 P. \tag{23}$$

D is an average diffusion constant. Solving Eq. (23) in the domain volume $V=\ell_x\ell_y\ell_z$ and using the solution for $P(\vec{r}',\vec{r},t')$ in Eq. (22) leads to

$$\langle \Delta Q_j^c(0,\vec{q}) \Delta Q_k^{c*}(t',\vec{q}) e^{i\vec{q}(\vec{r}-\vec{r}')} \rangle = \langle \Delta Q_j^c(0,\vec{q}) \Delta Q_k^{c*}(t',\vec{q}) \rangle I_x I_y I_z \tag{24}$$

with I_i given by

$$I_i = \sum_{n=1}^{\infty} e^{-D(n\pi/\ell_i)^2 t'} \frac{16\left(\frac{q_i \ell_i}{2\pi}\right)^2}{\pi^2 \left[n^2 - 4\left(\frac{q_i \ell_i}{2\pi}\right)^2 \right]} [1-(-1)^n] + \delta_{q_i,0}. \tag{25}$$

Molecular diffusion between neighboring domains is not included in the model as it is expected to be small compared to diffusion inside the domains. This hypothesis relies basically on the consideration that the number of molecules diffusing across the domain boundary is much lower than the number of molecules diffusing inside the domain, due to geometric reasons. Moreover, the diffusion constant on the domain boundary is expected to be smaller than inside the nematic domain due to energy barriers associated to the defects in the domain boundary [35]. Besides, the inclusion of this additional effect would substantially increase the number of fitting parameters in the model, far beyond the accuracy allowed by the available experimental data.

The correlation function for ΔQ_n^c can be obtained from the continuum theory of nematics as presented in [36,37] and detailed in the Appendix, the result is

$$\langle \Delta Q_n^c(0,\vec{q}) \Delta Q_l^{c*}(t',\vec{q}) \rangle = \sum_{m=1}^{5} P_{nm}(\vec{q}) P_{lm}(\vec{q}) \frac{kT}{V E_{mm}(\vec{q})} e^{-t'/\tau_m}, \tag{26}$$

where V is the nematic domain volume, T is the absolute temperature, k is the Boltzman constant, $E_{mm}(\vec{q})$ is the eigenvalue associated with the eigenmode m of the quadratic term of the free energy on the perturbation $\Delta Q_n^c(\vec{q})$ with wave vector $\vec{q}$, $P_{nm}(\vec{q})$ is the n,m term of the matrix whose columns are the eigenvectors associated with eigenvalues $E_{mm}(\vec{q})$, and τ_m is the decay time constant of eigenmode m.

The final expression for $\langle (X-\langle X \rangle)^2 \rangle$ is obtained using Eqs. (10), (11), (21), and (24)–(26) and becomes quite lengthy. However, the simpler form given below corresponds to the situation realized in our case where the correlation function for ΔQ_n^c given in Eq. (26) sharply decreases for q values away from zero and so only the $\vec{q}=0$ mode is important. In this situation diffusion inside each nematic domain does not affect the spectra, the I_i terms reduce to 1 and we obtain

$$\langle (X-\langle X\rangle)^2\rangle = c^2\left(\frac{3\pi}{\sqrt{6}}\frac{eQ}{h}\right)^2 \sum_{n,l=-2}^{2} G_n(\Omega)G_l(\Omega)\sum_{i,j=1}^{5} C_{ni}C_{lj} \times \sum_{m=1}^{5} P_{im}(\vec{q}=0)P_{jm}(\vec{q}=0)\frac{kT}{VE_{mm}(\vec{q}=0)} \times 2\tau_m[\tau_m e^{-t/\tau_m}(2e^{-\tau/\tau_m}-e^{-2\tau/\tau_m}) + 2\tau_m e^{-\tau/\tau_m} - 3\tau_m + t + 2\tau]. \quad (27)$$

The quantities $P_{nm}(\vec{q})$, $E_{mm}(\vec{q})$, $\tau_m(\vec{q})$ are calculated in the framework of the Landau–de Gennes (LG) free energy expansion on the order parameter tensor, considering terms up to sixth order to allow for the occurrence of biaxial nematic phases [36].

The LG free energy density expansion is

$$F(Q_{ij}) = F_0 + \tfrac{1}{2}A_0(T-T^*)Q_{ij}Q_{ji} + \tfrac{1}{3}BQ_{ij}Q_{jk}Q_{ki} + \tfrac{1}{4}C(Q_{ij}Q_{ji})^2 + \tfrac{1}{5}D(Q_{ij}Q_{ji})(Q_{ij}Q_{jk}Q_{ki}) + \tfrac{1}{6}[E(Q_{ij}Q_{jk}Q_{ki})^2 + E'(Q_{ij}Q_{ji})^3] + \tfrac{1}{2}(L_1Q_{ij,k}Q_{ij,k} + L_2Q_{ij,j}Q_{ik,k} + L_3Q_{ij,k}Q_{ik,j}), \quad (28)$$

where $F_0, A_0, T^*, B, C, D, E, E', L_1, L_2, L_3$ are constants [36,37] and summation over repeated indices is implied. The quantities $S(T), \eta(T), A_0, T^*, L_1, L_2, L_3$, are fitting parameters in the model. The quantities B, C, D, E, E', are set by A_0, T^* and the temperature dependencies of both the order parameter S and the asymmetry parameter η. A surface contribution to the free energy of the type proposed by Durand [38] and with a surface density of

$$f_s = \frac{G}{2}(Q_{ij}-Q_{ij}^s)^2, \quad (29)$$

where Q_{ij}^s is the desired order parameter tensor at the surface and G is a constant quantifying the surface interaction was also considered to account for the effects of the interdomain boundaries. Q_{ij}^s is identified with the average order parameter tensor in the nematic domain. The time dependence of the correlation function given in Eq. (26) was evaluated considering the dynamics of the order parameter in the nematic phase as described by Qiang and Sheng [39] and neglecting flow giving rise to the relaxation equation,

$$\gamma\frac{\partial \Delta Q_i^c(t,\vec{r})}{\partial t} = -\frac{\delta F}{\delta \Delta Q_i^c(t,\vec{r})}, \quad (30)$$

where γ is a viscosity coefficient as described in the Appendix.

The detailed evaluation of the quantities $P_{nm}(\vec{q}), E_{mm}(\vec{q}), \tau_m(\vec{q})$ is given in the Appendix.

When $G(\omega)$ [Eq. (6)] was actually fitted to data, an additional temperature-dependent line broadening was included through convoluting with a Lorentzian line-shape function to account for the presence of those collective modes that are almost static in the NMR measurement time.

IV. RESULTS AND DISCUSSION

A. Determination of ν_Q and η and the nematic order parameter S

The values of the averaged quadrupolar coupling constant ν_Q and the nematic order parameter S, and the asymmetry parameter η for the different temperatures studied were obtained by a simultaneous fit of 18 spectra corresponding to the six different temperatures studied and including the spectra recorded with the aligned sample, with the 90° rotated sample, and with the continuously rotating sample, using the approach described in Sec. III B. The simulated spectra using this procedure are shown along with the data in Figs. 4(a)–4(c). The resulting values for the nematic order parameter S, the asymmetry parameter η, and the quadrupolar coupling constant ν_Q as a function of the temperature are shown in Figs. 5(a) and 5(b) where the values reported in Ref. [8] are also included for comparison.

The approach designed to account for the presence of slow motions includes several other parameters beyond S (or ν_Q,) and η whose determination must be discussed. As mentioned before, the values of the parameters B, C, D, E, and E' associated to the Landau–de Gennes free energy expansion are determined by the S and η values at the six different temperatures studied and the values of A_0 and T^*. To decrease the number of free fitting parameters, A_0 was estimated independently from the *I-N* transition enthalpy and the value of the order parameter S just below the *I-N* transition [41] $(A_0 = 90\times 10^3\ \mathrm{J\,m^{-3}\,K^{-1}})$ T^* was considered to be within 1 K of the *I-N* transition temperature and one elastic constant approximation was considered $L \equiv L_1 = L_2 = L_3$. Five temperature-dependent mode viscosities $\gamma_i(T)$ also appear in the model, two of them associated with the dynamics of the $\boldsymbol{n}_1$ director reorientation were set equal, $\gamma_4(T) = \gamma_5(T)$. $\gamma_1(T)$ and $\gamma_2(T)$ associated with the dynamics of the fluctuations in the values of S and η are not important for the fits because the modes involved show a very low amplitude due to the high energy cost involved in changing either S or η from their equilibrium values, the relevant viscosities are then $\gamma_3(T)$ associated with the dynamics of the secondary directors reorientation and $\gamma_4(T) = \gamma_5(T)$. The surface interaction strength G and the domain volume V complete the list of parameters characterizing the model describing the presence of slow motions in the NMR time scale. Within the model used, the domain volume V is not determinable independently from G, L and the viscosities and only the products $(GV^{2/3})$, (LV), and $[\gamma_i(T)V]$ can be obtained from the fits. Besides, it was also found that, with values of L typical of liquid crystalline materials $(\sim 10^{-12}\ \mathrm{N})$ and $V = \ell^3$, with ℓ above one- tenth of a micron, the correlation function for ΔQ_n^c given in Eq. (26) only assumes significant values for $\vec{q}=0$. On the other hand, the elastic constant does not contribute to the term with $\vec{q}=0$ in the final expression for $\langle (X-\langle X\rangle)^2\rangle$ which is given in Eq. (27). Consequently, the product LV does not affect the fits in these conditions.

The products $(GV^{2/3})$ and $[\gamma_i(T)V]$ constitute the fitting parameters along with $S(T)$ [or $\nu_Q(T)$] and $\eta(T)$. Table I lists the value obtained for $(GV^{2/3})$ and Fig. 6 presents $[\gamma_3(T)V]$ and $[\gamma_4(T)V] = [\gamma_5(T)V]$. When analyzing the spectra in the

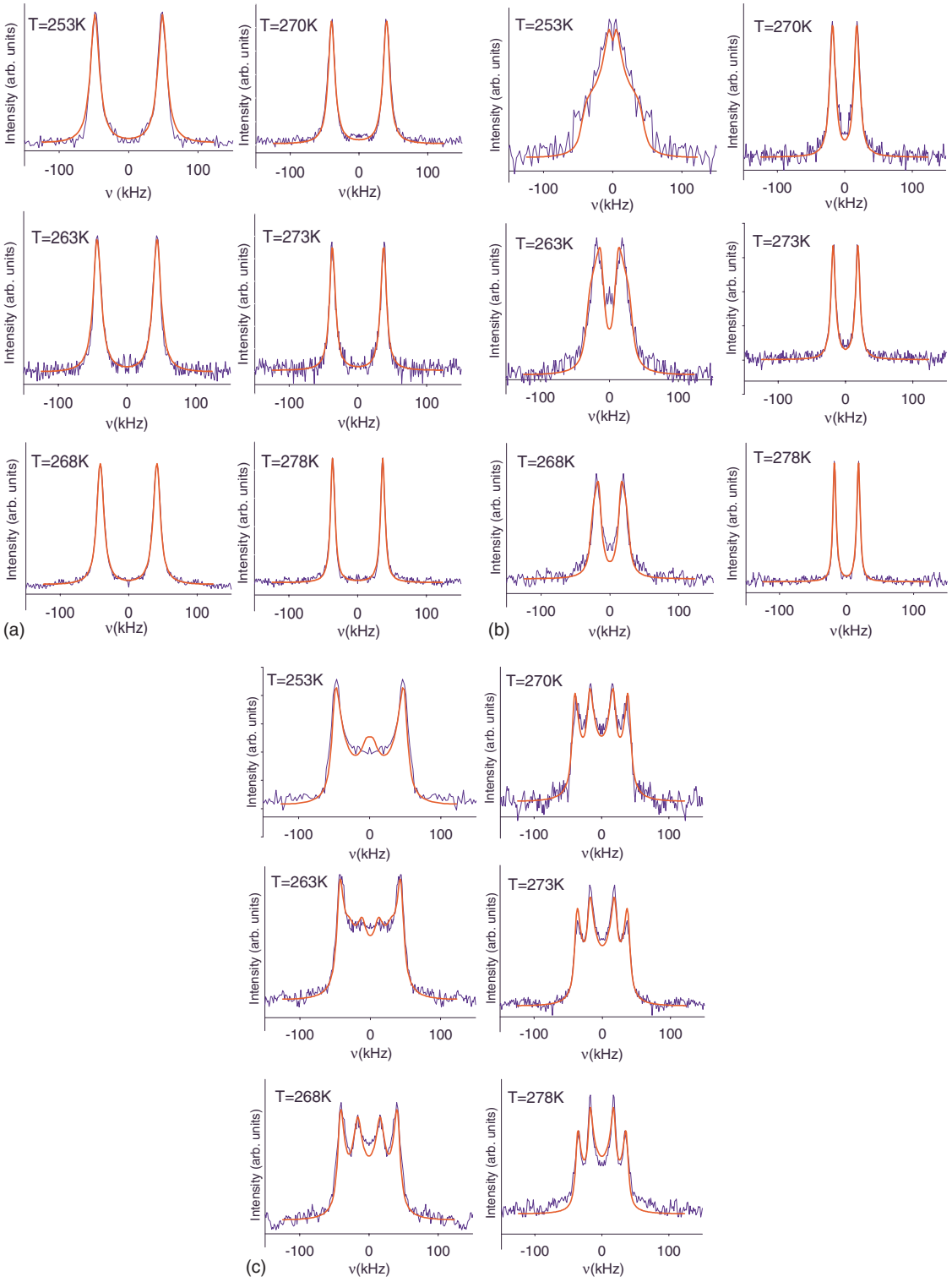

FIG. 4. (Color online) (a) Deuterium NMR spectra obtained at different temperatures for the aligned sample and fits. The fits result from a simultaneous fit of the data shown in (a)–(c). Experimental data, thin line; fits, thick line. (b) Deuterium NMR spectra obtained at different temperatures for the sample rotated of 90° about an axis perpendicular to the static magnetic field $\boldsymbol{B}_0$ and fits. Experimental data, thin line; fits, thick line. (c) Deuterium NMR spectra obtained at different temperatures for a continuously rotating sample about an axis perpendicular to the static magnetic field $\boldsymbol{B}_0$ and fits. Experimental data, thin line; fits, thick line.

biaxial nematic phase recorded with the sample either rotated 90° or in continuous rotation, the distribution of orientations of the secondary directors must be considered as detailed below. Distinct distributions of the secondary directors for the 90° rotated sample spectra and the continuous rotating sample spectra were included and parametrized through a Fourier expansion on the secondary director orientation angle.

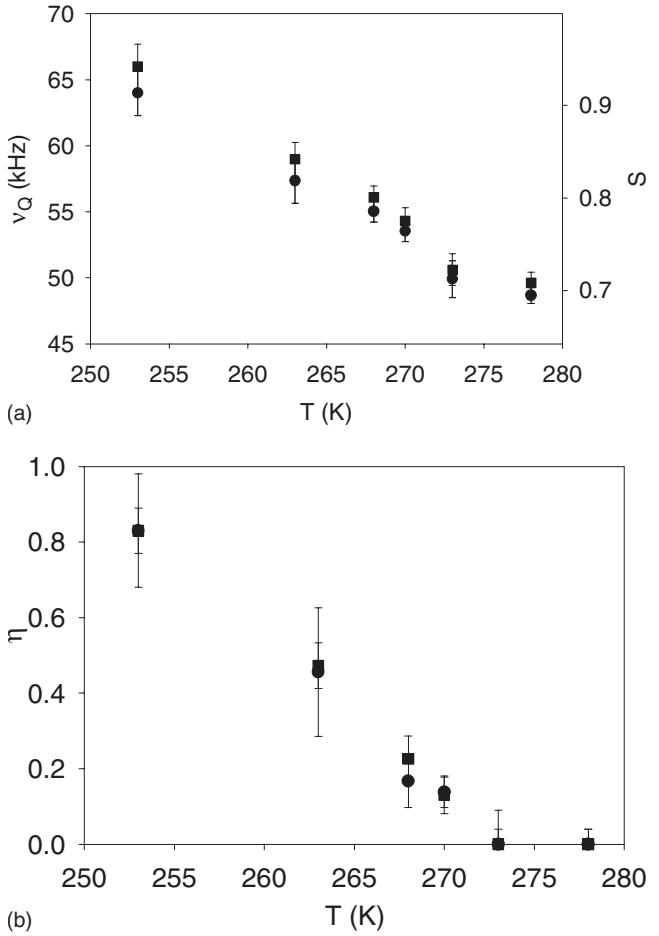

FIG. 5. (a) Temperature dependence of the averaged quadrupolar coupling constant ν_Q and the order parameter S obtained from the fits of expression (6) to the NMR spectra [presented in Figs. 4(a)–4(c)] represented by the square symbols and the ν_Q values (circles) obtained just from fits of the aligned sample data and the 90° rotated sample data disregarding slow molecular motions and reported in [8]. (b) Temperature dependence of the asymmetry parameter η obtained from the fits of expression (6) to the NMR spectra [presented in Figs. 4(a)–4(c)] represented by the square symbols and the η values (circles) obtained just from the fits of the aligned sample data and the 90° rotated sample data disregarding slow molecular motions and reported in [8].

1. Spectra recorded in the 90° rotated sample

Spectra recorded in the 90° rotated sample or in the continuous rotating sample are essential to measure the asymmetry parameter η. Equation (2) shows this very well since only when the main director n_1 is away from the static field B_0 direction ($\theta \neq 0$) the splitting becomes dependent upon the asymmetry parameter η. In this work both methods are used simultaneously to determine η and in this way allow more reliable values for η to be obtained.

TABLE I. Temperature independent fitting parameter considered in the model describing the slow modes contribution to the spectra.

$GV^{2/3}$ (J)
0.83×10^{-20}

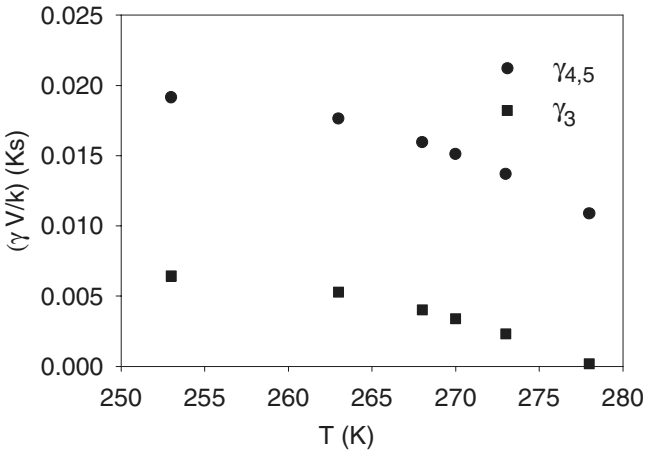

FIG. 6. Temperature dependence of the products of the mode viscosities γ_3 and $\gamma_4 = \gamma_5$ by the domain volume V. For convenience the values of these products are displayed divided by the Boltzman constant k.

The effectiveness of the 90° rotated sample method is clearly shown by the highest temperature spectra [see Fig. 4(b)]. Even in that case, which corresponds to the situation of easiest alignment breaking, it is easy to verify that the alignment is maintained through the whole sample. This is clearly confirmed by the characteristic reduction of the quadrupolar line splitting to one-half when the aligned sample is rotated by 90° in the uniaxial nematic phase.

In the biaxial phase, spectra recorded for the 90° rotated sample reflect the distribution of the $\boldsymbol{n}_2$ and $\boldsymbol{n}_3$ directors corresponding to the different domains in the sample. When biaxiality is present, a finite asymmetry parameter can give rise to a linewidth increase or to a partial powder pattern. In order to fit the spectra from the 90° rotated sample, a nonuniform distribution of the secondary directors around the main director was considered. This is compatible with a partial reorientation of the secondary directors induced by $\boldsymbol{B}_0$ in the rotated sample and does not conflict with the determination of the asymmetry parameter. This is the case because the partial powder patterns obtained allow for the simultaneous determination of the asymmetry parameter and the partial alignment distribution profile.

The distribution $P_0(\Omega)$ for the aligned sample expresses the alignment of the main directors with $\boldsymbol{B}_0$ and the uniform distribution of the secondary directors, and is given by

$$P_0(\Omega) = \frac{1}{\pi}\delta(\cos\theta - 1). \tag{31}$$

In the sample rotated by 90° the main director is orthogonal to $\boldsymbol{B}_0$ and the secondary directors are nonuniformly distributed in the plane perpendicular to $\boldsymbol{n}_1$. This situation is described by the distribution

$$P(\Omega) = \delta(\cos\theta)h(\varphi), \tag{32a}$$

where $h(\varphi)$ is given by

$$h(\varphi) = \begin{cases} [1 + C_1 \cos(2\varphi) + C_2 \cos(4\varphi) + C_3 \cos(6\varphi)]/C_0, & h(\varphi) \geqslant 0, \\ 0, & h(\varphi) < 0. \end{cases} \tag{32b}$$

C_0 is a normalization factor and C_1, C_2, and C_3 are temperature-dependent fitting parameters. This parametrization of $P(\Omega)$ is compatible with the symmetry of the magnetic contribution to the free energy of a nematic domain [36]. The ideal limiting situation of a perfectly aligned biaxial nematic monodomain sample would be described by

$$h(\varphi) = 1/2\delta[\cos^2(\varphi) - 1], \quad 0 \leqslant \varphi < 2\pi. \tag{32c}$$

From the analysis of the data presented in this work it was verified that the alignment conditions expressed by Eq. (32c) were not attained. Instead, a careful discussion on the biaxial ordering and domains distributions, based on the fitting of Eqs. (32a) and (32b) to our data, must be undertaken.

2. Spectra recorded in the continuous rotation experiment

The second type of experiment referred to in Sec. II B was performed on the same sample using the technique (continuous sample rotation) described in the literature [4,22,40]. In that method, the continuous rotation of the sample around one axis perpendicular to the NMR static magnetic field $\boldsymbol{B}_0$, as described in Sec. II B, generates a distribution of the $\boldsymbol{n}_1$ director. In this case, generally considered in the literature [22], a two dimensional powder pattern is formed as $\boldsymbol{B}_0$ lies distributed with equal probability in the plane defined by $\boldsymbol{n}_1$ and $\boldsymbol{n}_2$ [4,22,40] in the frame of the rotating sample. The case described above [4,22,40] implies a perfect alignment of one of the secondary directors ($\boldsymbol{n}_3$) of the biaxial nematic domains with the axis of the sample rotation. In our system the powder patterns obtained in the continuous rotation experiment show a clear difference relative to the usual two-dimensional (2D) powder patterns obtained in uniaxial and biaxial rotating nematics [4,22,40], and that difference becomes more pronounced as the temperature is lowered into the biaxial phase. It was also observed that the integral of the experimental spectra obtained with the rotating nematic is reduced relative to the aligned sample spectra.

When simulations of the spectra corresponding to the continuous rotating sample are attempted using the approach given in Sec. III A, the results presented in Fig. 7 (along with the data) are obtained. These simulations were prepared using the approach given by Eqs. (1) and (2) with a polarized distribution of secondary directors (associated with each domain) where $\boldsymbol{n}_3$ is aligned with the rotation axis and the values of ν_q and η reported in Figs. 5(a) and 5(b). As stated above, and could be anticipated, these simulations are not compatible with the data. Additional simulations, considering alternative distributions of the secondary directors (including the uniform distribution) and allowing also ν_Q and η to vary, were also unfitted to explain the experimental results.

The shape distortion and the decrease in area of the spectra from the continuous rotating sample are two factors that together can be caused by the combined effects of the presence of slow molecular motions and the use of the quadrupolar echo pulse sequence [27]. In order to simulate consistently the results of the aligned sample spectra, the 90° rotated sample spectra and the continuous rotated sample spectra, slow motions must be taken into account in the simulations as discussed in Sec. III B and shown in figures 4(a)–4(c). In carrying out the simulations for the continuous rotating sample, the domain orientation distribution in this case was also taken into account. As the signal acquisitions were unsynchronized with the sample rotation, a continuous planar distribution of $\boldsymbol{n}_1$ directors around an axis perpendicular to $\boldsymbol{B}_0$ was assumed (this is compatible with both a rotating aligned sample and a sample with a uniform $\boldsymbol{n}_1$ distribution in a plane perpendicular to the rotation axis). In the present case, it was verified by additional synchronized experiments that the uniform distribution of $\boldsymbol{n}_1$ correspond ef-

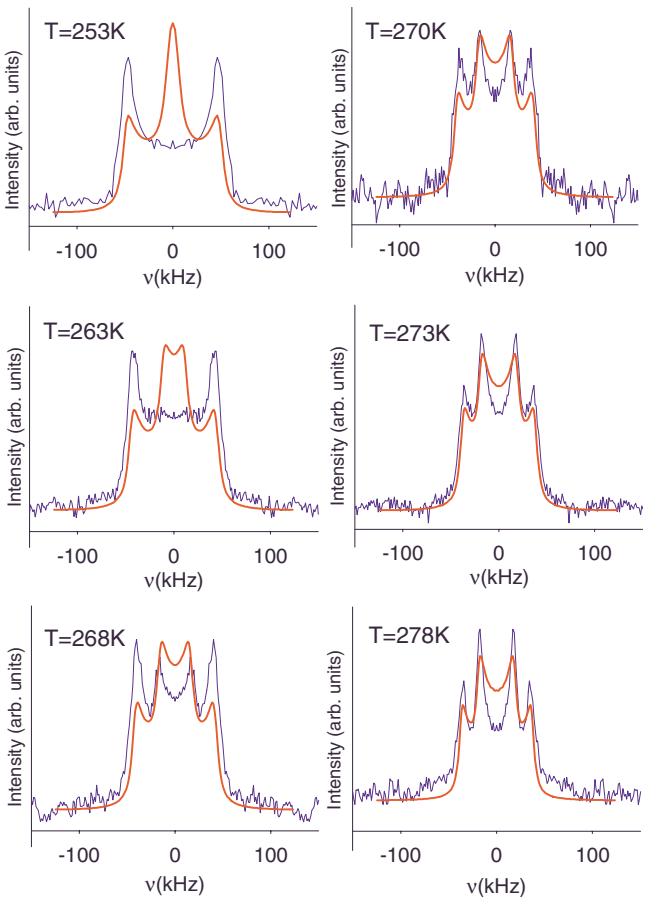

FIG. 7. (Color online) Deuterium NMR spectra registered from the continuously rotating sample at different temperatures and simulated spectra obtained with ν_Q and η reported in Figs. 5(a) and 5(b), disregarding slow molecular motions. Experimental data, thin line; simulation, thick line.

fectively to the rotation of the previously aligned sample [42]. The partial orientation of the secondary directors $\boldsymbol{n}_2$ and $\boldsymbol{n}_3$ express a polarized distribution in the frame associated to the initially aligned sample with a common $\boldsymbol{n}_1$, which is rotating around the axis perpendicular to $\boldsymbol{B}_0$. The orientation distribution of the secondary directors in the continuous rotating sample is parametrized by an expression identical to Eq. (32b) but with only one term in the series expansion due to the lack of sensitivity of the spectra to the presence of higher-order terms.

The spectra (thin lines) and the fits obtained considering the presence of slow motions (thick lines) appear as indicated before in figures 4(a)–4(c). These results correspond to the aligned sample (a), 90° rotated sample (b), and continuously rotating sample (c), respectively.

The discrepancy between the experimental data and the fits found when slow motions are disregarded in the continuous rotation spectra was corrected with the introduction of the slow reorientations of the principal axis frame of the electric field gradient tensor (associated with the C-D bond), averaged over fast motions, within a time scale similar to the NMR characteristic time (in this case the delay τ between the two pulses in the quadrupolar echo). Actually, the NMR signal expressed by Eqs. (4) and (6), tends to the static case described by Eq. (1) at the limits corresponding to

(i) movement with a time scale much larger then τ for which the principal axis of the AFG tensor may be considered at rest and is constant during the time τ;

(ii) movement with a time scale much smaller then τ for which a constant AFG tensor resulting from the averaging over fast movements is observed by NMR.

In both cases, $\langle (X-\langle X\rangle)^2\rangle \cong 0$ and expression (6) with $f(t)$ given by (4) is reduced to Eq. (1) corresponding to the static distribution. In the intermediate case, associated with movements of time scale comparable to τ the more detailed analysis described in Sec. III B must be followed.

The domain distributions considered for the 90° rotated sample spectra and for the continuous rotating sample spectra are shown in Figs. 8 and 9.

3. Discussion of the fit results

The values of ν_Q, S, and η obtained from the fits are, within experimental error, in good agreement with those reported in Ref. [8] resulting from an analysis where only aligned sample spectra and 90° rotated sample spectra were considered and slow motions were not taken into account, as can be seen in Figs. 5(a) and 5(b) where both data sets are shown. This is possible because the effect of the collective modes on the NMR spectra is more pronounced when the main director is away from the parallel or perpendicular orientations relative to B_0 due to the stationary behavior of $P_2(\theta)$ for $\theta=0$ and $\theta=\pi/2$. The compatibility between the fits for the 90° rotation sample experiment and the continuous rotating sample experiment (including slow motions), constitutes a strong experimental confirmation of the validity of values found for ν_Q, S, and η.

The domain orientation distribution $h(\varphi)$ is shown in Fig. 8 for the 90° rotated sample and in Fig. 9 for the continuous rotating sample for the different temperatures in the biaxial nematic phase.

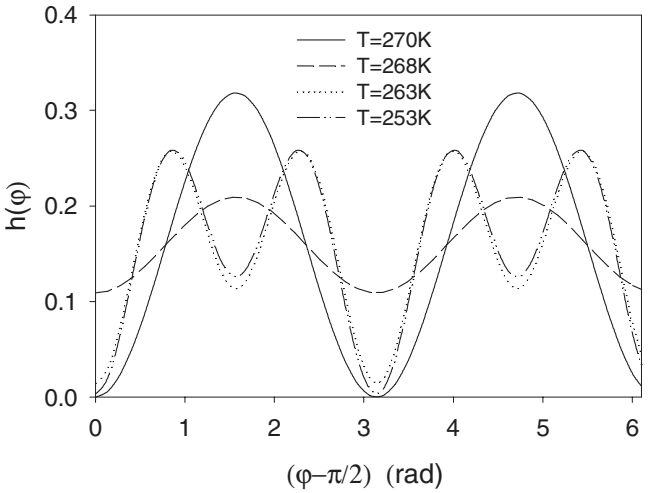

FIG. 8. Orientation distribution function of the secondary directors $h(\varphi)$ for the temperatures studied in the biaxial phase for the 90° rotated sample experiment. ($\varphi=\alpha_1+\pi/2$).

In the case of continuous rotation (Fig. 9) it is possible to observe a clear tendency of the secondary director $\boldsymbol{n}_3$ to align perpendicular to the magnetic field for increasing temperatures as could be expected. At the highest temperature of measurement, where $\eta>0$ (270 K), the secondary director $\boldsymbol{n}_3$ in the nematic domains is aligned, although imperfectly, perpendicular to the plane where the static magnetic field $\boldsymbol{B}_0$ evolves. For lowest temperatures the secondary directors corresponding to different nematic domains tend to be more equally distributed in the plane perpendicular to $\boldsymbol{n}_1$. At the lowest temperature of measurement, corresponding to the highest values of the asymmetry parameter, the distribution of secondary directors is practically uniform in the plane perpendicular to $\boldsymbol{n}_1$. It is important to remember that these distributions of $\boldsymbol{n}_2$ and $\boldsymbol{n}_3$ correspond to different domains all with a common alignment direction of $\boldsymbol{n}_1$. This set of do-

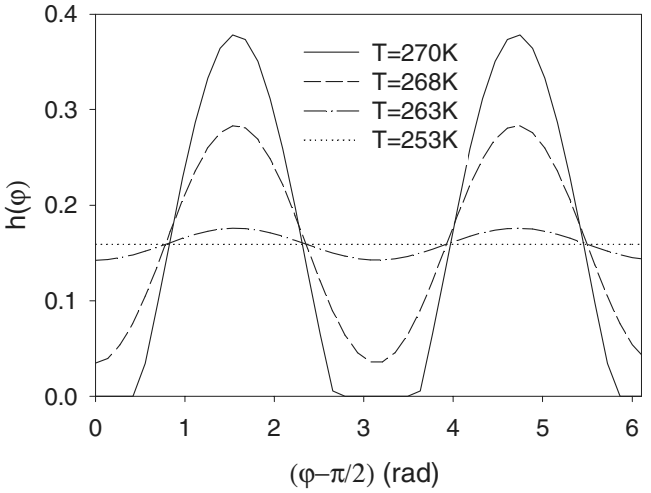

FIG. 9. Orientation distribution function of the secondary directors $h(\varphi)$ for the temperatures studied in the biaxial phase for the continuous rotating sample experiment.

mains is rotating coherently and the apparent distribution of $\boldsymbol{n}_1$ in the plane perpendicular to the rotation axis, correspond in fact to the accumulation of data scans at random angles resulting from the asynchrony between sample rotation and data acquisition [42].

The dependency of the secondary director distribution with temperature is more complex in the case of the 90° sample rotation technique. This could result from a competition between the decreasing of the viscosity with the increasing of temperature (which promotes the easiness of secondary director alignment), on the one hand, and the decreasing of the asymmetry parameter with the increasing of temperature (which promotes the tendency for a less anisotropic distribution, considering the corresponding decrease in the magnetic energy anisotropy), on the other hand. Nevertheless, for the highest measurement temperature with $\eta > 0$, the tendency of alignment of the secondary directors with the magnetic field is clear, although imperfect.

The temperature independent fitting parameter arising from the model of the slow molecular motions is given in Table I while Fig. 6 presents the dependent ones which are in this case the order parameter relaxation modes viscosities $\gamma_3(T)$ and $\gamma_4(T)=\gamma_5(T)$ multiplied by the domain volume V. To discuss the value reported in Table I we may consider a hypothetical domain volume corresponding to a characteristic length of the order of the tenths of a micron. With this hypothetical volume, the resulting mode viscosities obtained from the values presented in Fig. 6, are below the typical values of the rotational viscosity coefficient (γ_1) found for thermotropic liquid crystals what can be accounted for within the nematodynamics theory [36]. Regarding the surface energy coefficient G, a value of the order of 10^{-6} J m^{-2} is obtained within the same hypothesis.

From the values of the asymmetry parameter (measured in a bulk sample) it is possible to verify, within the experimental error, that the investigated system presents a nematic biaxial phase ($\eta > 0$) for temperatures below 273 K and a uniaxial nematic phase ($\eta = 0$) at and above this value. Notable for this system is that large values for the asymmetry parameter could be measured. This is attributed to the stability of the N_b phase at low temperatures in favor of higher-ordered LC phases. This could be a guide for the design of future materials. It is important to notice that the values of η measured in this work correspond to domains' distributions of the secondary directors all with a common principal director. The tendency of alignment of secondary directors with the increasing of temperature corresponds to an additional piece of information on the biaxial ordering of the system. Although a nematic biaxial monodomain was not observed, the measurement of an asymmetry parameter clearly different from zero and with considerably high values, far behind the limits of experimental error, for low temperatures along with partial alignment of the secondary directors induced by the magnetic field in both the continuous rotating sample and the 90° rotated sample, is an evidence of biaxial nematic ordering in these domains. The question of the size of the domains is not fully answered by the results presented although a domain size corresponding to a characteristic length of the order of the tenths of a micron has shown to be compatible to our results as referred before. The answer to the questions on the biaxial ordering of the phases exhibited by the material studied in this work may be better addressed by considering the contribution presented herein with others resulting from different experimental techniques. In fact the ^{2}H NMR experimental results presented here are essentially consistent with investigations of biaxiality on the same material (TM35) through the analysis of optical polarizing microscopy textures, conoscopy and polarized ir spectroscopy reported in [7] and also with results of dynamic light scattering on a similar compound reported in [43]. The difference between the uniaxial-biaxial transition temperatures obtained in the different studies is associated with the presence of the probe in the NMR sample (15% in weight) and the experimental error. Additionally, the different experimental geometries (bulk vs thin film) must be taken into account.

B. Discussion on the origin of the nematic phase biaxiality

The origin of the biaxiality evidenced by the results shown in the preceding section can be discussed in terms of the molecular structure of the tetrapodes and the resulting local structure of the nematic phase.

Several theoretical models and simulation studies have been used to describe the appearance of biaxial ordering in the nematic phase of different systems [1,11–14,44,45]. Earlier in the paper the Landau–de Gennes [36] expansion was used due to its simplicity and adequacy to quantify the effect of the collective modes on the NMR spectra, however to better describe the molecular order in the biaxial nematic phase other approaches have been used including models relying on the Saupe order matrices $S^i_{\alpha\beta} = \langle \frac{1}{2}(3\cos\theta_{i\alpha}\cos\theta_{i\beta} - \delta_{\alpha\beta})\rangle$, where $i=X,Y,Z$ refers to the axis of the phase frame (the Z axis of this frame is coincident with the principal director $\mathbf{n}_1$ in each nematic domain) and $\theta_{i\alpha}$ $\theta_{i\beta}$ are the angles between the axis of phase frame and those of the molecular frame, α, $\beta = x,y,z$. Following the approach of Straley [44] the elements of the AFG tensor in the phase frame [that determine the value of the asymmetry parameter given by Eq. (3)] can be expressed in terms of the components of the average electric field gradient tensor associated to the C-D bond in the molecular frame (V_{ii} $i = x,y,z$) by means of four order parameters, S, D, P, and C,

$$\bar{V}^{ZZ} = \frac{D}{3}(V_{xx} - V_{yy}) + SV_{zz}, \tag{33a}$$

$$\bar{V}^{XX} - \bar{V}^{YY} = \frac{C}{3}(V_{xx} - V_{yy}) + PV_{zz}, \tag{33b}$$

where the order parameters are given by

$$S \equiv S^Z_{zz} = \left\langle \frac{3}{2}\cos^2\beta - \frac{1}{2} \right\rangle, \tag{34a}$$

$$D \equiv S^Z_{xx} - S^Z_{yy} = \left\langle \frac{3}{2}\sin^2\beta\cos 2\alpha \right\rangle, \tag{34b}$$

$$P \equiv S^X_{zz} - S^Y_{zz} = \left\langle \frac{3}{2}\sin^2\beta\cos 2\gamma \right\rangle, \tag{34c}$$

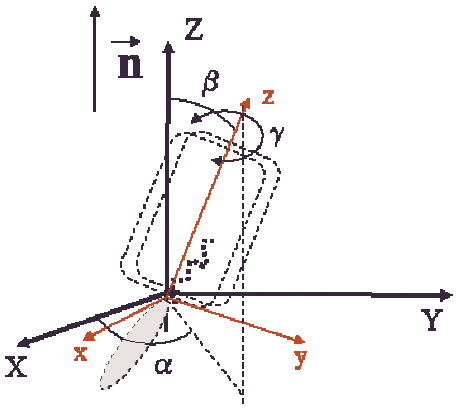

FIG. 10. (Color online) Angles between the phase (*XYZ*) and molecular (*xyz*) frames used in the definition of the *S*, *D*, *C*, and *P* order parameters.

$$C \equiv (S_{xx}^X - S_{yy}^X) - (S_{xx}^Y - S_{yy}^Y) = \left\langle \left(\frac{3}{2}\cos^2\beta + \frac{1}{2} \right) \cos 2\alpha \cos 2\gamma - 3\cos\beta \sin 2\alpha \sin 2\gamma \right\rangle. \quad (34d)$$

β is the angle between the molecular z axis and the Z axis of the phase frame; α is the azimuthal angle with respect to the X axis defined by the projection of the z axis on the XY plane; γ is the angle associated with rotations of the molecular frame around the z axis (see Fig. 10). S is the nematic order parameter and is a measure of the tendency of the z molecular axis to align with the principal director defined by the Z phase axis. D is a molecular asymmetry parameter that measures a difference of tendency of the main director (defined by phase axis Z) projection in the xy plane to align with respect to axes x and y of the molecular frame. This parameter may be understood as a measure of the molecular "flatness" in a uniaxial phase [37]. P is a biaxiality parameter that measures the difference of the tendency of the z molecular axis projection in the XY plane to align with the X and Y axis, respectively. Finally C is an intrinsic (molecular) biaxiality parameter for a biaxial phase.

Now, the origin of the experimental values found for the asymmetry parameter η may be discussed taking into account Eqs. (3), (33), and (34) and considering the meaning of the different order parameters. Equations (33) show that the asymmetry parameter results from two contributions, one proportional to the phase biaxiality parameter, P, and another proportional to the molecular biaxiality parameter C. As can be seen in Eqs. (34c) and (34d), these two contributions are of different nature and may be understood as resulting (i) from the anisotropy of the fluctuations of orientation of the most ordered molecular axis (z) in the XY phase plane; (ii) from the hindering of the rotational movements of the molecule around the most ordered molecular axis. As an example it may be referred that in smectic phases of tilted molecules (e.g., SmC, SmF), the phase biaxiality P generally dominates and a biaxial phase may be formed by molecules of cylindrical symmetry. Contrary, in a nematic phase, especially in a highly ordered nematic (which is clearly the case investigated here for the very low temperatures where the asymmetry parameter reaches very high values) the low amplitude of fluctuations in β ($\sin\beta \to 0$) results in a low contribution from the effect of the anisotropy of the fluctuations of orientation of the most ordered molecular axis (z) in the XY phase plane, (i). Therefore, it must be expected that the contribution (ii) from the hindering of rotations around the most ordered molecular axis dominates. Consequently, molecular biaxiality must be present together with reasons for anisotropic molecular rotational movements around the z axis in order to explain the high values of the asymmetry parameter, η obtained at low temperatures in the case studied here.

The molecular packing in this nematic phase was studied in previous investigations by means of x-ray diffraction and polarized ir spectroscopy and it was confirmed that, as discussed before (see Fig. 2), the phase structure is characterized by the interdigitation of interconnected mesogenic units belonging to different tetrapodes [16–18]. The importance of this type of molecular interdigitated packing on the molecular dynamics has been confirmed by proton NMR relaxometry [16]. Clearly, these mesogenic units are strongly restricted with respect to rotations around their long molecular axis through their lateral covalent link to the alkyl/siloxane chain which connects to the central siloxane core. According to Eqs. (33b) and (34d) biaxiality must result mainly from the anisotropy of molecular rotations in the angle γ corresponding to reorientations around the long molecular axis. Jointly there must be some anisotropy of the AFG tensor in the molecular frame with respect to the xx and yy components. These can be explained through the constraints imposed on the probe by local molecular packing of the tetrapodes resulting on asymmetrical fluctuations of the C-D bond.

In summary, it can be stated that the tetrapodes, which form a monodisperse system of supermolecular interdigitated plates, as shown in Fig. 2, originate a biaxial nematic phase at low temperatures due to the hindering of molecular movements around the most ordered molecular axis. This effect has some similarities with that observed by NMR on a side-on thermotropic nematic polymer as reported in [5]. In that case biaxiality is also presented as a consequence of the hindering of rotations of the mesogenic units as due to the lateral attachment to the polymer chain. However, the system described in this work is a monodisperse supermolecular system, with a clear overall geometry, where biaxiality is immediately evident through the observation the NMR spectra. Also the values of the asymmetry parameter found for the biaxial nematic phase of the tetrapode studied in this work are quite high (see Fig. 5) and clearly far above those observed for bent-core mesogens [4] or the thermotropic nematic polymer [5]. As discussed in [8], the very low temperatures, where the biaxial nematic phase of the tetrapode (mixed with 7CBαd2) appears, provide a strong supporting argument for this result. As observed by Berardi and Zannoni [46], using Monte Carlo simulations where biaxiality of the molecules and of their interactions is considered, with decreasing of the temperature, the tendency for the occurrence

of a biaxial nematic phase competes with the propensity for the onset of a more ordered phase (generally a smectic phase). In our case, the special characteristics of the molecular structure of the tetrapodes give rise to a nematic phase over a very large temperature range allowing for the appearance of the biaxial nematic order. Indeed, a simple model where hindering of rotations on the angle γ is taken into account in the calculation of the AFG tensor clearly leads to such high values of the asymmetry parameters. This effect occurs for low temperatures, just provided that the potential barrier associated with the hindering of the rotations becomes important when compared to the available thermal energy [8]. In addition to the fast local hindered molecular reorientations resulting in a biaxial average field gradient tensor (clearly shown by the very high asymmetry parameter values), slow molecular motions were also detected in this investigation. The latter can be associated with slow collective modes of the nematic phase [16,24,31]. The hypothesis that the biaxial nematic ordering observed in domains with different orientations of secondary directors is related with the hindering of rotations around the direction defined by $\boldsymbol{n}_1$ is compatible with the observation of the curves for the secondary directors distributions presented in Figs. 8 and 9. In fact, as the temperature decreases the ordering associated with $\boldsymbol{n}_2$ and $\boldsymbol{n}_3$ in each domain becomes higher and higher as shown by the increasing values of η, but simultaneously the common ordering of these domains becomes less and less effective. This fact, which may be macroscopically described as an effect of the increase of rotational viscosity in the material, may be associated to the conjecture that, at lower temperatures, the increasing of the biaxial ordering in each domain corresponds to a higher energetic cost for the mutual reorientation between domains.

The experimental manipulation of the material in order to obtain a biaxial nematic monodomain is a question that deserves further research work. The standard procedure of cooling the system from the isotropic phase to the measurement temperature in the presence of the static NMR magnetic field is ideal for eliminating defects in the distribution of the main director. However, for symmetry reasons it is useless to align the secondary directors. The repeated tilting technique, which was used in this work for the measurement of the spectra in the 90° rotated samples has shown not to be sufficiently effective for the preparation of a biaxial nematic monodomian, especially for low temperatures. From the observation of the curves in Figs. 8 and 9 it may be conjectured that cooling the sample from a previously aligned situation at a temperature in the biaxial nematic phase would lead to further aligned samples at lower temperatures. However, it is not clear how the defects corresponding to the secondary directors distributions will behave along the process. The fact that the observation of the secondary directors' distribution is not direct and depends on a detailed posterior analysis of the measured spectra increases the experimental difficulties of obtaining such an ideal sample preparation. In any case, the measurement of values of the asymmetry parameter in polydomain samples with partial alignment of secondary directors is a clear indication of biaxial ordering in the nematic domains.

V. CONCLUSION

The presence of a biaxial nematic phase in an organosiloxane tetrapode polydomain sample was observed by means of two independent ^{2}H NMR experiments. Both procedures used (90° rotation and continuous rotation) correspond to well-established techniques for sample handling during NMR measurements, particularly adequate for the analysis of biaxial ordering in liquid crystal phases [2,4,8,22,23]. The biaxial nematic mesophase is detected for temperatures below 0 °C, confirming results presented recently on this thermotropic monodisperse system [8]. The use of the nematic liquid crystal 7CBαd2 as a deuterated probe (15% in weight) was shown to be particularly effective in the detection of nematic biaxiality. This was expected as the interactions between the phenyl rings of the probe and those of the tetrapode mesogenic units favor the ordering of the probe as a result of the molecular packing of the host. The values of ν_Q, S, and η resulting from the coherent use of the two distinct methods in this investigation confirm those previously reported. It must be noted that the values of these parameters obtained in this experiment correspond to the mixture of tetrapode with the nematic LC used as a deuterated probe. Nevertheless, the fact that the probe used is clearly uniaxial indicates that the biaxiality of the system originates from the tetrapodes nematic arrangement. The particularly high values of the asymmetry parameter obtained for low temperatures are interpreted as a consequence of the specific molecular structure of the tetrapodes [8]. The existence of a nematic phase ranging to such low temperatures and the hindering of the local reorientational movements of the tetrapodes contribute to the high values of η in agreement with a model presented in [8]. In addition, slow molecular movements are evidenced by the line-shape analysis of the spectra resulting from the continuously rotating sample. Consistent values for the fitting parameters ν_Q and η are obtained for the two experiments when the presence of slow molecular motions in the time scale of the NMR measurement is taken into account. In fact, the consideration of the presence of the slow molecular motions (associated with collective modes of the nematic phase) proved to be essential to the simulation of the continuous rotating sample spectra particularly in the lower temperatures analyzed. Finally, it is important to note that the high values of the asymmetry parameter measured correspond to the nematic biaxial ordering in a polydomain sample with an overall common main director $\boldsymbol{n}_1$ and partial orientation of secondary directors $\boldsymbol{n}_2$ and $\boldsymbol{n}_3$. The perfect alignment of a NMR sample forming a single biaxial nematic monodomain of the organosiloxane tetrapode studied in this work is a possibility that depends on both the material properties and experimental conditions and deserves further investigation.

ACKNOWLEDGMENTS

This work was partially supported by the Portuguese Science Foundation (FCT) Contract Nos. POCTI/34453/CTM/2000, POCI/CTM/61293/2004, and PTDC/FIS/65037/2006 and by the EU through Contract No. HPRN-CT-2000-0016.

APPENDIX

Here, we give a detailed calculation of expression (26) and of the quantities $P_{nm}(\vec{q})$, $E_{mm}(\vec{q})$, $\tau_m(\vec{q})$. The first step is to decompose Q_{ij} as the sum of an average value plus a fluctuating part as in (13),

$$Q_{ij}(\vec{r}) = Q^0_{ij} + \Delta Q_{ij}(\vec{r}) \tag{A1}$$

and insert the result in F and f_s [Eqs. (28) and (29)] keeping terms only up to second order in the fluctuating part $\Delta Q_{ij}(\vec{r})$ since it is supposed to be small compared to the average value of Q. Next the $\Delta Q_{ij}(\vec{r})$ terms in F are renamed according to (18) and replaced by their spatial Fourier series and the free energy density is integrated over the volume of the nematic domain yielding the free energy of the domain $\mathcal{F}$. (The surface integral of f_s is converted to a volume integral using the divergence theorem with the contribution of nondiagonal terms neglected.) The domain free energy $\mathcal{F}$ becomes

$$\mathcal{F} = \mathcal{F}^0(Q^0) + \frac{V}{2}\sum_{\vec{q}} (\alpha_{ij} + q_k q_l \beta_{ikjl}) \Delta Q^c_i(\vec{q}) \Delta Q^{c*}_j(\vec{q}), \tag{A2}$$

where V is the domain volume and α_{ij} and β_{ikjl} are functions of the parameters A_0, B, C, D, E, E', $L \equiv L_1 = L_2 = L_3$, G, the temperatures T and T^* and the order parameter tensor Q^0. The indices i, j run from 1 to 5 and the indices k, l run from 1 to 3. The second term in $\mathcal{F}$ can be set in a diagonal form

$$\mathcal{F} = \mathcal{F}^0(Q^0) + \frac{V}{2}\sum_{\vec{q}} \Delta Q^c_i(\vec{q}) P_{in} (\delta_{nm} E_{mm}) P^{-1}_{mj} \Delta Q^{c*}_j(\vec{q}), \tag{A3}$$

where P_{in} is a matrix whose columns are the eigenvectors of the matrix with elements $(\alpha_{ij} + q_k q_l \beta_{ikjl})$ and E_{mm} are the eigenvalues of that matrix. δ_{nm} is the Kronecker δ symbol. The equipartition theorem allows us to write

$$\langle \Delta Q^c_i(\vec{q}) P_{in} P^{-1}_{nj} \Delta Q^{c*}_j(\vec{q}) \rangle = \frac{kT}{V E_{nn}} \tag{A4}$$

(with implied summation in the indices i and j but not n), that gives

$$\langle \Delta Q^c_i(\vec{q}) \Delta Q^{c*}_j(\vec{q}) \rangle = P^{-1}_{ni} P_{jn} \frac{kT}{V E_{nn}} \tag{A5}$$

(with implied summation in n).

The dynamics of the fluctuating part of Q is evaluated neglecting flow according to [39]

$$\gamma \frac{\partial \Delta Q^c_i(t,\vec{r})}{\partial t} = -\frac{\delta F}{\delta \Delta Q^c_i(t,\vec{r})} = -\left(\frac{\partial F}{\partial [\Delta Q^c_i(t,\vec{r})]} - \partial_k \frac{\partial F}{\partial [\Delta Q^c_{i,k}(t,\vec{r})]} \right) \tag{A6}$$

which correspond to the Landau-Kalatnikov equations for the dynamics of the order parameter. Replacing in the previous equation $\Delta Q^c_i(t,\vec{r})$ by its Fourier series expansion we obtain

$$\gamma \frac{\partial \Delta Q^c_i(t,\vec{q})}{\partial t} = -(\alpha_{im} + q_k q_l \beta_{ikml}) \Delta Q^c_m(t,\vec{q}) \tag{A7}$$

that can be set in the form

$$\gamma_i \frac{\partial}{\partial t} P^{-1}_{im} \Delta Q^c_m(t,\vec{q}) = -E_{ii} P^{-1}_{in} \Delta Q^c_n(t,\vec{q}), \tag{A8}$$

where we have introduced a different γ value for each mode and summation is implied in the indices m and n. The equation integrates to give

$$\Delta Q^c_m(t,\vec{q}) = P_{mi} e^{-(E_{ii}/\gamma_i)t} P^{-1}_{in} \Delta Q^c_n(0,\vec{q}). \tag{A9}$$

Consequently the correlation function $\langle \Delta Q^c_m(0,\vec{q}) \Delta Q^{c*}_l(t,\vec{q}) \rangle$ is given by

$$\langle \Delta Q^c_m(0,\vec{q}) \Delta Q^{c*}_l(t,\vec{q}) \rangle = P_{li} P_{ni} e^{-E_{ii}/\gamma_i t} \langle \Delta Q^c_m(0,\vec{q}) \Delta Q^{c*}_n(0,\vec{q}) \rangle = P_{li} P_{ni} e^{-E_{ii}/\gamma_i t} P^{-1}_{km} P_{nk} \frac{kT}{V E_{kk}} \tag{A10}$$

that simplifies to

$$\langle \Delta Q^c_m(0,\vec{q}) \Delta Q^{c*}_l(t,\vec{q}) \rangle = P_{lk} P_{mk} e^{-E_{kk}/\gamma_k t} \frac{kT}{V E_{kk}} \tag{A11}$$

which is expression (26) with

$$\tau_k = \frac{\gamma_k}{E_{kk}}. \tag{A12}$$

[1] M. J. Freiser, Phys. Rev. Lett. **24**, 1041 (1970).

[2] G. R. Luckhurst, Thin Solid Films **393**, 40 (2001); Nature (London) **430**, 413 (2004).

[3] R. Berardi, L. Muccioli, and C. Zannoni, J. Chem. Phys. **128**, 024905 (2008).

[4] L. A. Madsen, T. J. Dingemans, M. Nakata, and E. T. Samulski, Phys. Rev. Lett. **92**, 145505 (2004); B. R. Acharya, A. Primak, and S. Kumar, *ibid.* **92**, 145506 (2004).

[5] K. Severing and K. Saalwächter, Phys. Rev. Lett. **92**, 125501 (2004).

[6] V. Channabasaveshwar, Y. S. K. Prasad, G. G. Nair, I. S. Shashikala, D. S. S Rao, C. V. Lobo, and S. Chandrasekhar, Angew. Chem., Int. Ed. **43**, 3429 (2004).

[7] K. Merkel, A. Kocot, J. K. Vij, R. Korlacki, G. H. Mehl, and T. Meyer, Phys. Rev. Lett. **93**, 237801 (2004).

[8] J. L. Figueirinhas, C. Cruz, D. Filip, G. Feio, A. C. Ribeiro, Y. Frère, T. Meyer, and G. H. Mehl, Phys. Rev. Lett. **94**, 107802 (2005).

[9] P. H. J. Kouwer and G. H. Mehl, J. Am. Chem. Soc. **125**, 11172 (2003); D. Apreutesei and G. H. Mehl, Chem. Commun.

(Cambridge) **2006**, 609 (2006).
[10] E. Date and D. W. Bruce, J. Am. Chem. Soc. **125**, 9012 (2003).
[11] A. Stroobants and H. N. W. Lekkerkerker, J. Phys. Chem. **88**, 3669 (1984).
[12] A. G. Vanakaras and D. J. Photinos, Mol. Cryst. Liq. Cryst. Sci. Technol., Sect. A **299**, 65 (1997); A. G. Vanakaras, S. C. McGrother, G. Jackson, and D. J. Photinos, *ibid.* **323**, 199 (1998); A. G. Vanakaras, A. F. Terzis, and D. J. Photinos, *ibid.* **362**, 67 (2001).
[13] P. Palffy-Muhoray, J. R. De Bruyn, and D. A. Dunmur, J. Chem. Phys. **82**, 5294 (1985).
[14] R. Blaak, B. M. Mulder, and Daan Frenkel, J. Chem. Phys. **120**, 5486 (2004).
[15] G. R. Newkome, C. N. Moorefield, and F. Vögtle, *Dendrimers and Dendrons, Concepts, Syntheses, Applications* (Wiley-VCH, Weinheim, 2001).
[16] D. Filip, C. Cruz, P. J. Sebastião, A. C. Ribeiro, T. Meyer, and G. H. Mehl, ECLC2003, Jaca, Spain.
[17] P. H. J. Kouwer, G. H. Mehl, ECLC2003, Jaca, Spain, Book of Abstracts.
[18] K. Merkel, A. Kocot, J. K. Vij, G. H. Mehl, and T. Meyer, J. Chem. Phys. **121**, 5012 (2004).
[19] J. Barberá, M. Marcos, and J. L. Serrano, Chem.-Eur. J. **5**, 1834 (1999).
[20] S. M. Fan, I. D. Fletcher, B. Gundogan, N. J. Heaton, G. Kothe, G. R. Luckhurst, and K. Praefke, Chem. Phys. Lett. **204**, 517 (1993).
[21] J. K. Hughes, G. Kothe, G. R. Luckhurst, J. Malthête, M. E. Neubert, I. Shenouda, B. A. Timini, and M. Tittlebach, J. Chem. Phys. **107**, 9252 (1997).
[22] F. P. Nicolettat, G. Chidichimo, A. Golemme, and N. Picci, Liq. Cryst. **10**, 665 (1991).
[23] J. L. Figueirinhas and J. W. Doane, Mol. Cryst. Liq. Cryst. Sci. Technol., Sect. A **238**, 61 (1994).
[24] K. Merkel, A. Kocot, J. K. Vij, G. H. Mehl, and T. Meyer, Phys. Rev. E **73**, 051702 (2006).
[25] S. Diez, D. Dunmur, M. R. De La Fuente, P. Karahaliou, G. H. Mehl, T. Meyer, M. A. Perèz Jubindo, and D. Photinos, Liq. Cryst. **30**, 1021 (2003); R. Elsasser, G. H. Mehl, J. W. Goodby, and D. J. Photinos, Chem. Commun. (Cambridge) **2000**, 851 (2000); T. Meyer and G. H. Mehl, The synthesis and the liquid crystal properties of Germanium containing multipodes, 19th International Liquid Crystal Conference, Edinburgh, UK, 2002.
[26] J. Figueirinhas, S. Zumer, and J. W. Doane, Phys. Rev. A **35**, 4389 (1987).
[27] H. W. Spiess and H. Sillescu, J. Magn. Reson. (1969-1992) **42**, 381 (1981).
[28] Y. Galerne, Mol. Cryst. Liq. Cryst. Sci. Technol., Sect. A **323**, 211 (1998).
[29] A. Abragam, *The Principles of Nuclear Magnetism* (Clarendon, Oxford, 1961).
[30] D. Frezzato, G. Kothe, and G. J. Moro, J. Phys. Chem. B **105**, 1281 (2001); D. Frezzato, G. J. Moro, and G. Kothe, J. Chem. Phys. **119**, 6931 (2003); D. Frezzato, G. Kothe, and G. J. Moro, *ibid.* **119**, 6946 (2003).
[31] R. Y. Dong, *Nuclear Magnetic Resonance of Liquid Crystals*, 2nd ed. (Springer-Verlag, Berlin, 1997).
[32] D. M. Brink and G. R. Satchler, *Angular Momentum* (Clarendon, Oxford, 1968).
[33] C. A. Veracini, in *Nuclear Magnetic Resonance of Liquid Crystals*, edited by J. W. Emsley, NATO ASI SERIES Series C: Mathematical and Physical Sciences Vol. 141 (D. Reidel, Dordrecht, Boston, Lancaster, 1983).
[34] B. Halle and S. Gustafsson, Phys. Rev. E **56**, 690 (1997).
[35] J. L. Figueirinhas, A. Ferraz, A. C. Ribeiro, F. Noack, and H. T. Nguyen, J. Phys. II **7**, 79 (1997).
[36] P. G. de Gennes and J. Prost, *The Physics of Liquid Crystals* (Oxford University Press, Oxford, 1993).
[37] G. Vertogen and W. H. de Jeu, *Thermotropic Liquid Crystals, Fundamentals* (Springer-Verlag, Berlin, 1988).
[38] M. Nobili and G. Durand, Phys. Rev. A **46**, R6174 (1992).
[39] Tiezheng Qian and Ping Sheng, Phys. Rev. E **58**, 7475 (1998).
[40] Louis A. Madsen and E. T. Samulski, Liq. Cryst. **32**, 1419 (2005).
[41] Matthew L. Magnuson, B. M. Fung, and J. P. Bayle, Liq. Cryst. **19**, 823 (1995).
[42] A. Van-Quynh, C. Cruz, G. Feio, A. C. Ribeiro, J. P. Casquilho, J. L. Figueirinhas, D. Apreutesei, T. Meyer, and G. H. Mehl, ILCC2006 Book of Abstracts, 2006.
[43] K. Neupane, S. W. Kang, S. Sharma, D. Carney, T. Meyer, G. H. Mehl, D. W. Allender, Satyendra Kumar, and S. Sprunt, Phys. Rev. Lett. **97**, 207802 (2006).
[44] J. P. Straley, Phys. Rev. A **10**, 1881 (1974).
[45] D. W. Allender, M. A. Lee, and N. Hafiz, Mol. Cryst. Liq. Cryst. **124**, 45 (1985); F. Biscarini, C. Chiccoli, P. Pasini, F. Semeria, and C. Zannoni, Phys. Rev. Lett. **75**, 1803 (1995); W. Li and K. F. Freed, J. Chem. Phys. **103**, 5693 (1995); M. C. J. M. Vissenberg, S. Stallinga, and G. Vertogen, Phys. Rev. E **55**, 4367 (1997); B. Mettout, P. Toledano, H. Takezoe, and J. Watanabe, *ibid.* **66**, 031701 (2002); H. H. Wensink, G. J. Vroege, and H. N. W. Lekkerkerker, *ibid.* **66**, 041704 (2002); A. M. Sonnet, E. G. Virga, and G. E. Durand, *ibid.* **67**, 061701 (2003); A. G. Vanakaras, M. A. Bates, and D. J. Photinos, Phys. Chem. Chem. Phys. **5**, 3700 (2003); M. A. Bates and G. R. Luckhurst, Phys. Rev. E **72**, 051702 (2005); L. Longa, P. Grzybowski, S. Romano, and E. Virga, *ibid.* **71**, 051714 (2005); B. Mettout, *ibid.* **72**, 031706 (2005).
[46] R. Berardi and C. Zannoni, J. Chem. Phys. **113**, 5971 (2000).